2.4. Wind loading

2.4.1. Single-point wind field The wind forces can be treated as a single-point if the size of gusts λ is large enough compared to the typical dimension D of the structure ($\lambda / D >> 1$), which means that the wind velocity field is assumed to be fully correlated. This assumption is quite valid for structures with small spatial size (Kareem and Dalton, 1982). The wind force on the platform using single-point formulation is given by:

$$F(t) = \frac{\rho_a C_D A_p U^2(t)}{2} \tag{6}$$

in which $U(t) = u(z) + u'$; A_p is the tower projected area above MSL. The mean wind load is given by:

$$\overline{F} = \frac{\rho_a C_D A_p u^2(z)}{2} \tag{7}$$

and the fluctuating wind force is given by:

$$F(t) = \rho_a C_D A_p u(z) u'(t) \tag{8}$$

2.4.2. Multiple-point wind field For large offshore articulated towers, full correlation assumption is impractical and may give conservative results under aerodynamic loads. Therefore, in such cases, multi-point-statistics is employed to incorporate the effects of partial correlation (Kareem and Dalton, 1982). The multi-point simulation means that the fluctuating wind velocity varies along the projected area. A Spatio-temporal function defines the fluctuating wind field as:

$$U(y,z,t) = u(z) + u'(y,z,t) \tag{9}$$

in which $u(z)$ is the mean wind, and $u'(y,z,t)$ the two-dimensional Spatio-temporal fluctuating wind.

The fluctuating with wind force in surge direction on the platform area A_p is given by:

$$F_a(y,z,t) = \rho_a C_d \int_{A_p} u(z) \int u'(y,z,t)\, dydz \tag{10}$$

For evaluating Eq. (10) the wind velocity is to be simulated at n locations on the tower deck. Then, Eq. (10) is discretized as:

$$F_a(y,z,t) = \rho_a \sum_{i=1}^{n} C_{d_i} A_i u(z) u_i'(t) \tag{11}$$

in which A_i and C_{d_i} are the segmental area and drag coefficient, i represents the i^{th} segment and $u_i'(t)$ the simulated fluctuating velocity at the i^{th} segment.

2.4.3. Dynamic force due to wind loading After modeling the wind field either by single- or multiple-point, the velocity field is transformed into the aerodynamic loading. The wind force per unit projected area of the tower deck is given by:

$$F_a(y,z,t) = 0.5\rho_a C_p(y,z)[u(z) + u'(y,z,t) - \dot{x}(t)]^2 \quad (12)$$

here $F_a(y,z,t)$ is the force per unit area, varies in space and time coordinates, ρ_a the air density; $C_p(y,z)$ the pressure coefficient at a height z and horizontal coordinate y; $\dot{x}$ the structural velocity in the surge direction; $u(z)$ the mean wind velocity, and $u'(y,z,t)$ the fluctuating wind velocity.

2.5 Wave loading

Modified Morison's equation has been employed to estimate the hydrodynamic load. The force on the member of j^{th} tower at i^{th} location due to fluid-structure interaction is given by:

$$F_h(t) = 0.5\rho_w C_D D_{ji}\left(\dot{u}_{fi} - r_{ij}\theta_j + v_c\right)\left|\dot{u}_{fi} - r_{ij}\theta_j + v_c\right| + \frac{\pi}{4}C_M \rho_w \pi D_{ji}^2 \ddot{u}_{fi} \pm \frac{\pi}{4}\rho_w D_{ji}^2 (C_M - 1) r_{ij}\ddot{\theta}_j \quad (13)$$

where C_D and C_M are drag and inertia coefficients; v_c is the velocity of current; D_{ji} is the diameter of the j^{th} tower for i^{th} element; r_{ij} is the distance of the i^{th} element from the hinge of the j^{th} tower. $\dot{u}_{fi}$ and $\ddot{u}_{fi}$ are the water particle velocity and acceleration normal to the displaced j^{th} tower at i^{th} location; θ_j is the tilt angle of the j^{th} tower and ρ_w is the mass density of seawater. The last term in Eq. (13) is due to the added mass. The positive sign is used when sea surface elevation η is below the mean sea level and vice-versa.

The sea surface is assumed to be a Gaussian-ergodic process. In contrast, the sea surface elevation is assumed to be a superposition of infinite small harmonic waves having a randomly distributed phase. The PSDF of sea surface elevation is a graphical representation of the energy content of various harmonics present in it. Here, the DNV version of the Pierson-Moskowitz spectrum is used.

$$S_\eta = \frac{H_s^2 T_z}{8\pi^2}(T_z f)^{-5} \exp\left[-\frac{1}{\pi}(T_z f)^{-4}\right] \quad (14)$$

where f is the frequency (cycles/sec); H_s is the significant wave height (m), T_z is the wave period (sec), and S_η is the P-M sea surface elevation spectrum.

3. GENERATION OF TIME HISTORY RESPONSE

The time histories of articulated tower displacement are generated by the Wilson-θ method. Time histories of responses must be of sufficient length so that r.m.s responses attain the steady-state values. In this study, the simulated length of time histories is taken as three hours. The transition phase of the oscillation, which is about 10 times the time period of the structure, has been ignored. For all the responses, the structure is assumed to be initially at rest. The time histories are obtained at a time interval of 0.7 sec. The PSDF of the responses is obtained by direct Fourier transform of the response time histories using a fast Fourier Transformation technique (FFT).

4. NUMERICAL STUDY

The dynamic response of a double-hinged articulated tower under single- and multiple-point wind field simulation has been carried out in a water depth of 420 m. The two segments idealized tower with a lumped mass at the top is used in the present investigation (see Fig. 1). Each segment is divided into 50 elements. The length of the bottom and top tower are taken as 260 m and 210 m, respectively. The structural mass of each shaft of the tower is taken as 200 KN/m. The deck and ballast mass are taken as 25000 KN and 448.4 KN/m, respectively. The position of buoyancy chamber from the mid hinge is taken as 135 m. The following data represents a tower for which the effective diameters of the shaft for drag, the buoyancy, and the added mass, as well as inertia, are 17 m, 7.5 m, and 4.5 m, respectively. Likewise, the same effective diameters for the buoyancy chamber are 20 m, 19.5 m, and 7.5 m. For the double-hinged tower, the natural frequencies were found as ω_1 =0.14 rad/sec (first mode) and ω_2 = 0.42 rad/sec (second mode) using the developed source code DHALP (Double Hinged Articulated Loading Platform). The code was developed using FORTRAN Power Station.

The characteristics of sea states are given in Table 1, whereas the wind characteristics are presented in Table 2. Detail of nonlinearities considered in the study is given in Table 3. The details of various components on the deck are shown in Fig. 4. For plotting PSDFs, the wind fluctuations are represented by Ochi and Shin wind spectrum. The wind spectra corresponding to wind velocities of 25 m/sec and 15 m/sec are shown in Fig. 5. The sea states corresponding to these wind velocities are labeled as high sea state (18.0 m, 13.6 sec) and moderate sea state (6.5 m, 8.15 sec).

Table 1 Characteristics of sea states

Wind velocity (m s^{-1})	wave height H_s (m)	Wave period T_z (sec)	Wave frequency (rad/sec)	Sea state designation
25	18.0	13.6	0.29 rad/sec	High sea state
15	6.50	8.15	0.55 rad/sec	Moderate sea state

Table 2 Wind characteristics

Parameter	Value
Wind drag coefficient	1.81
Mean wind velocity	15 and 25 m/sec
Air density	1.27 kg/ m^3
Reference elevation, z_{ref}	33.0 m
Equivalent area of tower superstructure	1557 m^2

A uniform current velocity of 1.0 m/sec is adopted in the analysis. The drag and inertia coefficients are assumed as 0.6 and 2.0. In order to satisfy the ergodicity, the duration of simulated time histories is taken as 3 hours, with a sampling interval of 0.7 sec. The

results for deck displacement, upper hinge roration, central hinge shear, and bending moment are summarized in Tables 4 and 5, respectively, for high and moderate sea states. Salient PSDFs are shown in Figs. 6- 9.

Table 3 Types of nonlinearities

Nonlinearities	Details of nonlinearities
Geometric nonlinearities	Large difference in the diameter of the buoyancy chamber and the tower's shaft
Force nonlinearities	Wave force introduces nonlinearity due to • Fluctuating buoyancy • Variable added mass • Instantaneous tower orientation

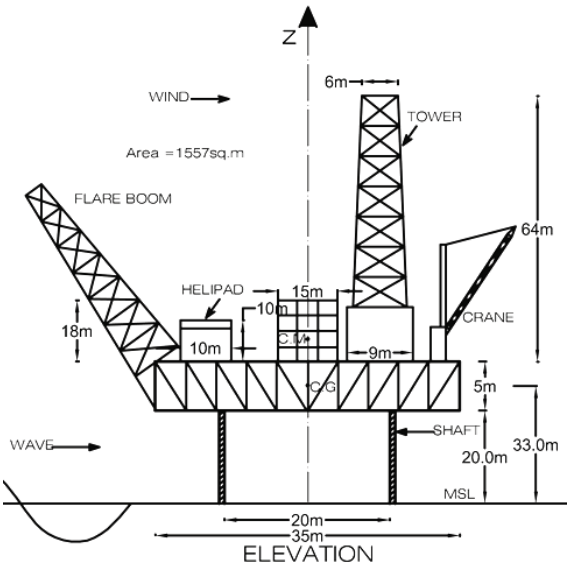

Fig. 4 Full scale dimensions of tower superstructure

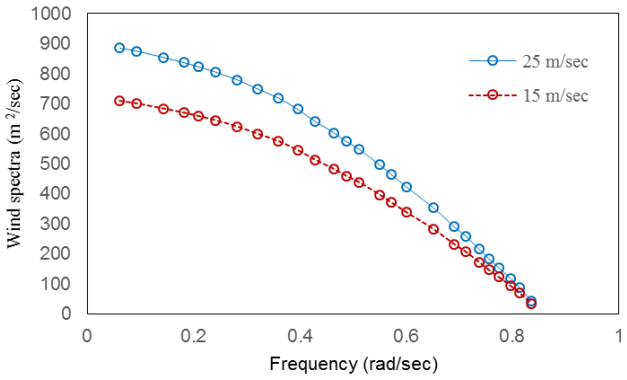

Fig. 5 Ochi and Shin spectra plot for different wind velocities

5. DISCUSSION OF RESULTS

5.1. Response under high sea state (H_s=18.0 m, T_z=13.6 sec)

Table 4 presents the RMS and maximum response of the tower for single-point and multiple-point wind field simulation for deck displacement, hinge rotation, hinge shear, and bending moment, respectively. When the multiple-point simulation is used, the RMS and maximum deck displacement response are reduced by 3.40% and 24.44%, respectively. Further, statistical results show that multiple-point analysis results in response estimates, which are generally lower than the single-point formulation, where

the full correlation is tacitly assumed over the entirety of the structure. PSDF of the deck displacement response under high sea state is shown in Fig. 6. Two significant peaks characterize the response spectra. The first peak occurs near the vicinity of the first natural frequency (0.14 rad/sec) of the tower, while the second peak occurs at the towers second frequency (0.42 rad/sec). It is also seen that the application of multiple-point wind field simulation brings down the peak of the PSDF at salient frequencies. The smaller peaks in between these higher peaks are the characteristic of a non-linear articulated tower system. Because of stress reversals, hinge shear in the articulated joints causes fatigue. Therefore, its systematic evaluation is critical for the safety and survival of the tower. The statistical quantities for central hinge shear in Table 4 are reduced by 3.60%, and 12.93%, respectively, which signifies the importance of multiple-point wind field simulation. The PSDF of bending moment under high sea state is presented in Fig. 7. Two appreciable peaks appear in the response PSDF. The first most prominent peak occurs at a low frequency (0.06 rad/sec), showing the influence of wind on the bending moment response. The second peak occurs at the tower's first frequency. Similar to deck displacement response, multi-point analysis decreases the spectral energy to a large extent at respective frequencies.

Table 4 Comparison of responses under high sea state

Responses ↓ Statistics →	RMS			Maximum		
	Single-point	Multiple-point	Decrease in response (%)	Single-point	Multiple-point	Decrease in response (%)
Deck displacement (m)	11.2	10.8	3.4	16.2	12.2	24.4
Upper hinge rotation (rad.)	3.8×10^{-2}	3.7×10^{-2}	3.1	5.9×10^{-2}	4.9×10^{-2}	17.7
Central hinge shear (N)	2.5×10^{7}	2.4×10^{7}	3.6	4.9×10^{7}	4.3×10^{7}	12.9
Bending moment (Nm)	4.4×10^{10}	4.2×10^{10}	5.2	-1×10^{11}	-1×10^{11}	5.55

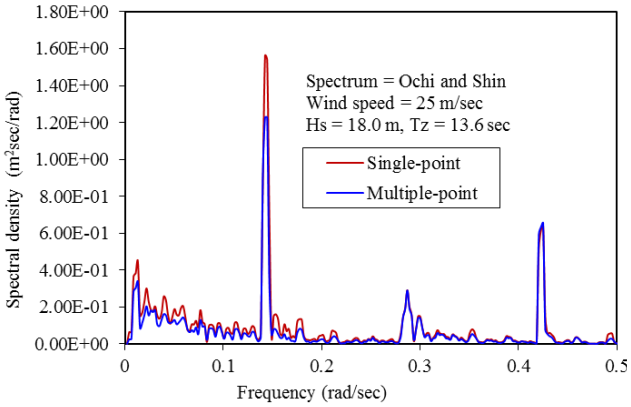

Fig. 6 PSD of surge response under high sea state

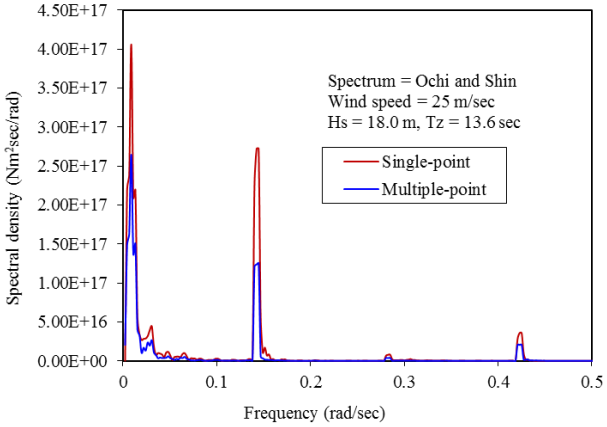

Fig. 7 PSD of bending moment response under high sea state

5.2 Response under moderate sea state (H_s=6.50 m, T_z=8.15 sec)

The PSDF of deck displacement under moderate sea state, as shown in Fig.8, is depicted by two prominent peaks. The first not so significant peak appears at a low-frequency, which corresponds to the peak frequency of the wind spectrum. The second spectral peak occurs at the first natural frequency of the tower (0.14 rad/sec). By comparing the deck displacement response under both wind simulations, it is seen that multi-point analysis significantly influences the deck displacement response of double articulated towers.

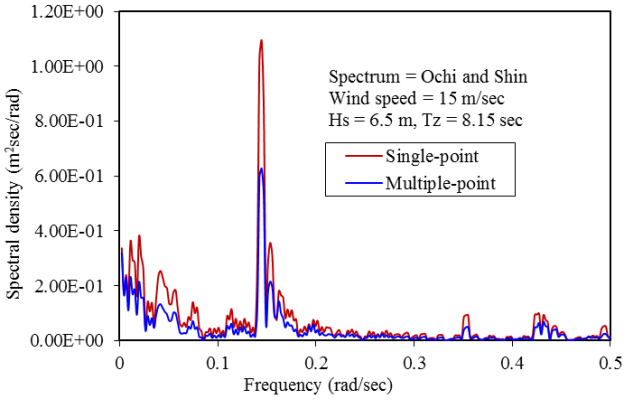

Fig. 8 PSD of surge response under moderate sea state

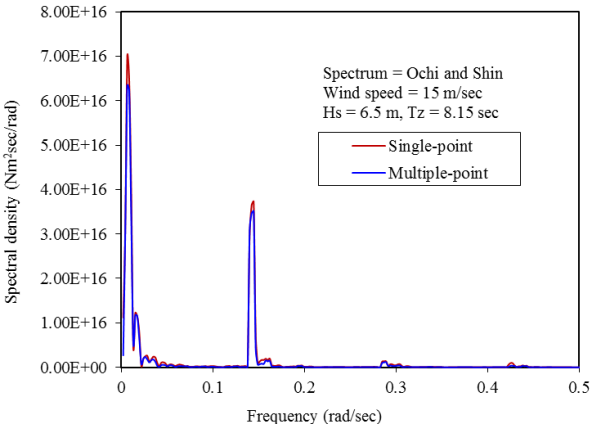

Fig. 9 PSD of bending moment response under moderate sea state

Table 5 Comparison of responses under moderate sea state

Responses ↓ Statistics →	RMS			Maximum		
	Single-point	Multiple-point	Decrease in response (%)	Single-point	Multiple-point	Decrease in response (%)
Deck displacement (m)	4.1	4.0	1.5	6.4	5.5	13.0
Upper hinge rotation (rad.)	1.4×10^{-2}	1.4×10^{-2}	1.4	2.6×10^{-2}	2.4×10^{-2}	5.8
Central hinge shear (N)	9.5×10^{6}	9.2×10^{6}	3.2	2.3×10^{7}	2.3×10^{7}	2.1
Bending moment (Nm)	1.5×10^{10}	1.4×10^{10}	5.8	-3.6×10^{10}	-3.4×10^{10}	6.1

Table 5 shows that multiple-point simulation lowers the RMS and maximum responses by 1.47% and 13.02%, respectively. Hinge shear response quantities in Table 5 under multi-point simulation are reduced by 3.24% and 2.15%, respectively. PSDF of bending moment response for moderate sea state is characterized by two peaks, as shown in Fig. 9. The second peak occurs at the tower's first frequency, which is not as significant as the first one. A decrease of about 6% is observed in RMS and maximum bending moment response while considering the effect of multiple-point wind simulation (Table 5).

6. CONCLUSIONS

From the dynamic analyses of the double-hinged articulated tower, it can be concluded that tower response is sensitive to the dynamic effects of wind. The multiple-point analysis results in response quantities, which are generally lower than the single-point formulation. The RMS and maximum response in the deck displacement are reduced by 3.40% and 24.44%, respectively when the multiple-point formulation is used under high sea state. The same response is reduced by 1.5% and 13.0% under moderate sea state. Therefore, it is argued that a conservative estimate of responses under single-point simulation can be effectively mitigated by using the multi-point formulation of wind loads, which results in the economical, safe, and reliable design of the tower. The energy content of PSDFs under multiple-point wind field is altered as compared to that with single-point simulation. It implies the significance of wind field simulation on the dynamics of a double-hinged tower. The distribution of energy against frequencies provides valuable data used in the design of a non-linear articulated tower system.

7. REFERENCES

Antoniou, M., Gelagoti, F. and Anastasopoulos, I. (2019), "A compliant guyed system for deep-sea installations of offshore wind turbines: Concept, design insights and dynamic performance." *Soil Dynamics and Earthquake Engineering*, Vol. **119**, 235–252.

Aslam, M. Islam. N. zaheer, M.M. and Alam, M. (2013a), "Behaviour of double pendulum loading platform under ocean." *International Journal of Innovative Research in Science, Engineering and Technology*, Vol. **2**(6), 2145–2152.

Aslam, M. Islam. N. zaheer, M.M. and Alam, M. (2013b), "Comparative Response of Double Hinged Alp Using Airy ' S and Stokes ' Wave Theories." Vol. **2**(5), 1532–1539.

Bar-Avi, P. and Benaroya, H. (1996), "Response of a two degrees of freedom articulated tower to different environmental conditions." *International Journal of Non-Linear Mechanics*, Vol. **31**(5), 717–741.

Bisht, R. S. and Jain, A. K. (1998), "Wind and wave induced behaviour of offshore guyed tower platforms." *Ocean Engineering*, Vol. **25**(7), 501–519.

Chandrasekaran, S. and Madhuri, S. (2015), "Dynamic response of offshore triceratops: Numerical and experimental investigations." *Ocean Engineering*, Vol. **109** 401–409.

Chandrasekaran, S., Madhuri, S. and Jain, A. K. (2013), "Aerodynamic response of offshore triceratops." *Ships and Offshore Structures*, Vol. **8**(2), 123–140.

Chandrasekaran, S. and Nassery, J. (2017), "Non-linear response of stiffened triceratops under impact and non-impact waves." *Ocean Systems Engineering*, Vol. **7**(3), 179–193.

Datta, T. K. and Jain, A. K. (1990), "Response of articulated tower platforms to random wind and wave forces." *Computers & Structures*, Vol. **34**(1), 137–144.

Eyada Ibrahim, A. and Jameel, M. (2018), "Wind Induced Response of Spar-mooring-riser System." *KSCE Journal of Civil Engineering*, Vol. **22**(8), 2653–2663.

Fang, C., Li, Y. and Chen, X. (2019), "Extreme Response of a Sea-Crossing Bridge Tower under Correlated Wind and Waves." *Jr. of Aerospace Engg.*, Vol. **32**(6), 1–13.

Fang, C., Li, Y. and Wei, K., (2019), "Vehicle–bridge coupling dynamic response of sea-crossing railway bridge under correlated wind and wave conditions." *Advances in Structural Engineering*, Vol. **22**(4), 893–906.

Ghorai, B., Selvam, P. and Sundaravadivelu, R. (2015), "Hydrodynamic Responses of a Single Hinged and Double Hinged Articulated Tower." OMAE 2015-41524, *Proceeding of OMAE*. Newfoundland, Canada.

Islam, A. B. M. S. *et al.* (2012), "Review of offshore energy in Malaysia and floating Spar platform for sustainable exploration." *Renew Sustain Energy Reviews*, Vol. **16**(8), 6268–6284.

Islam, N., Zaheer, M. M. and Ahmed, S. (2009), "Response of double hinged articulated tower platforms to wind forces." *Wind and Structures, An International Journal*, Vol. **12**(2). 103-120.

Kareem, A. (1985), "Wind-Induced Response Analysis of Tension Leg Platforms." *Journal of Structural Engineering*, Vol. **111**(1), 37–55.

Kareem, A. *et al.* (1987), "Aerodynamic loads on a typical tension leg platform." *Ocean Engineering*, Vol. **14**(3), 201–231.

Kareem, A. and Dalton, C. (1982), "Dynamic Effects of Wind on Tension Leg Platforms."

Proceeding of *Offshore Tech. Conference*. Houston, Texas, 235–242.
Kushal Solomon, D. K. (2019), "Optimal Control for Response Reduction of Single Hinged Articulated Tower Using MR-Damper." Proceeding of OMAE2019-96076. **Vol. 3**, Glasgow, Scotland, UK
Lamei, A. and Hayatdavoodi, M. (2020), "On motion analysis and elastic response of floating offshore wind turbines." *Journal of Ocean Engineering and Marine Energy*, Springer International Publishing, Vol. **6**(1), 71–90.
Li, Y. and Kareem, A. (1990), "Stochastic response of tension leg platforms to wind and wave fields." *Journal of Wind Engineering and Industrial Aerodynamics*, Vol. **36**, 915–926.
Myrhaug, D. (2007), "Wind gust spectrum over waves: Effect of wave age." *Ocean Engineering*, Vol. **34**, 353–358.
Nagavinothini, R. and Chandrasekaran, S. (2019), "Dynamic analyses of offshore triceratops in ultra-deep waters under wind, wave, and current." *Structures*, **20**, 279–289.
Ormberg, H., Baarholm, R. and Stansberg, C. T. (2003), "Time-domain coupled analysis of deepwater TLP, and Verification against Model Tests." *ISOPE Conference*. Hawaii, USA, 145–152.
Oyejobi, D. O., Jameel, M. and Ramli Sulong, N. H. (2016), "Non-linear response of tension leg platform subjected to wave, current and wind forces." *International Journal of Civil Engineering*. Vol. **14**(8), 521–533.
Philip, V., Joseph, A. and Joy, C. M. (2015), "Three Legged Articulated Support for 5 MW Offshore Wind Turbine." *Aquatic Procedia*. Elsevier B.V., **4**, 500–507.
Roy R. Craig (1983), *Structural Dynamics: An Introduction to Computer Methods*, International. John Wiley and Sons, (WIE).
Zaheer, M.M. and Islam, N. (2008), "Aerodynamic response of articulated towers: State-of-the-art." *International Journal of Wind and Structures*, Vol. **11**(2), 97–120.
Zaheer, M. M. and Islam, N. (2008), "Fluctuating wind induced response of double hinged articulated loading platform." *OMAE 2008, Proc 27th Int Conference On Offshore Mechanics Arctic Engineering,* 2008, Estoril, Portugal, Vol. **1**, 723–731.
Zaheer, M. M. and Islam, N. (2010), "Reliability analysis of universal joint of a compliant platform." *Fatigue and Fracture of Engineering Materials and Structures*, Vol. **33**(7), 408–419.
Zaheer, M. M. and Islam, N. (2017), "Dynamic response of articulated towers under correlated wind and waves." *Ocean Engineering*. Elsevier, Vol. **132**, 114–125.
Zaheer, M. M. and Islam, N. (2020), "Effect of current on the dynamic response of a bi-articulated offshore tower." *Advances in Structural Engineering*, 1–13.
Zeng, X., Liu, Y., Shen, X. and Wu, Y. (2006), "Non-linear dynamic response of tension leg platform." *ISOPE Conference*, 94–100. Lisbon, Portugal.
Zhang, B. L., Han, Q. L. and Zhang, X. M. (2017), "Recent advances in vibration control of offshore platforms." *Nonlinear Dynamics*. Springer Netherlands, Vol. **89**(2), 755–771.

NOMENCLATURE

L_1	length of the lower shaft
L_2	length of the top shaft

r_{2j}	position vector of an element in the top tower measured from the mid hinge
θ_1	hinge rotation of the lower shaft
θ_2	hinge rotationof the top shaft
F_θ	Forcing function due to environmental loads at any instant of time
I_{1t}	moment of inertia of the lower shaft
I_{2t}	moment of inertia of the top shaft
$\overline{m}_{2t}$	mass of the top tower
m_a	added mass of the structure
m_2	mass of the top shaft
m_{ac}	time-invariant added mass upto MSL
m_{af}	fluctuating added mass
m_d	mass of the deck
I_d	moment of inertia of the deck
L_p	height of c.g of the deck above mid hinge
P_{cm}	height of c.g above the deck
F_1	buoyancy force in the lower shaft
F_2	buoyancy force in the top shaft
W_1	weights of the lower shaft
W_2	weights of the upper shaft
W_d	weight of the deck
b_2	center of buoyancy in the upper shaft from mid hinge
c_2	center of mass in the lower shaft from mid hinge
F_a	aerodynamic force
F_d	fluid drag force
F_i	fluid inertia force
C_p	wind pressure coefficient
$\dot{x}$	structural velocity in the horizontal direction
u	mean wind velocity
u'	fluctuating wind velocity
A_a	projected area of the tower normal to the wind flow
$u(z_{ref})$	reference velocity at a height of 10 m above MSL
$S(f_i)$	spectral density of one sided sea surface elevation spectrum at the frequency f_i